Turbulence Decay and Restratification in the Equatorial Ocean Surface Layer following Nighttime Convection

D. R. CALDWELL

College of Oceanic and Atmospheric Sciences, Oregon State University, Corvallis, Oregon

R.-C. LIEN

Applied Physics Laboratory, University of Washington, Seattle, Washington

J. N. MOUM

College of Oceanic and Atmospheric Sciences, Oregon State University, Corvallis, Oregon

M. C. GREGG

Applied Physics Laboratory, University of Washington, Seattle, Washington

(Manuscript received 5 December 1995, in final form 18 November 1996)

ABSTRACT

Although the process of restratification of the ocean surface layer at the equator following nighttime convection is similar in many ways to the process at midlatitudes, there are important differences. A composite day calculated from 15 days of consistent conditions at 140°W on the equator was compared with midlatitude observations by Brainerd and Gregg. In the depth range of 20–40 m, 1) minimum nighttime stratification was similar [N^2 of 1.2–3.2 ($\times 10^{-6}$ s^{-2}) vs 0.4–1.7 ($\times 10^{-6}$ s^{-2})], 2) maximum daytime stratification was significantly larger, as might be expected from the greater surface heat input [N^2 of 8–21 ($\times 10^{-6}$ s^{-2} vs 3–7 ($\times 10^{-6}$ s^{-2})], and 3) minimum nighttime shear was similar [shear-squared was 1.4–4.6 ($\times 10^{-6}$ s^{-2}) vs 0.8–1.9 ($\times 10^{-6}$ s^{-2})], but the maximum daytime shear was much larger [shear-squared of 24–41 ($\times 10^{-6}$ s^{-2}) vs 3–7 ($\times 10^{-6}$ s^{-2})].

For much of the surface layer, the dominant identifiable cause of restratification in both cases was the divergence of the penetrating shortwave radiation, although at the equator the divergence of turbulent flux was important from 10 to 25 m. In both cases the divergence of vertical fluxes accounted for only 60%–70% of the restratification; relaxation of lateral gradients was probably the source for the rest. At the equator, the shear in the upper 40 m was restored in the daytime by turbulent transport of momentum injected by the wind.

In the region convectively mixed at night, turbulence decayed exponentially in the daytime in both cases, the *e*-folding time, τ_ε, being 1.7 ± 0.2 h at the equator, 1.5 h in midlatitude. A dimensionless decay time, $N\tau_\varepsilon$, was 7.2–9.3 compared with 6.0 in the midlatitude case. In both cases the vertical scale of the turbulence was controlled by the Ozmidov scale, and the turbulence remained active throughout the day.

At the equator ''deep-cycle'' nighttime turbulence was generated in the always-stratified water at depth 60–80 m never reached by nighttime convection. Neither shear nor stratification varied significantly diurnally. The decay of this turbulence was similar to that above in that its vertical scale was controlled by the Ozmidov scale and remained active throughout the day, but the *e*-folding timescale was much longer, 3.5 h ($N\tau_\varepsilon$ = 66–96). For the turbulence to persist this long, turbulence production must be a large proportion of ε.

1. Introduction

In midlatitudes, the diurnal cycle of turbulence in the ocean surface layer plays an important role in determining vertical transports of heat, mass, and momentum. Frequently nighttime surface cooling drives turbulent convective transport to depths well below those reached by turbulence driven only by wind stress. In this convective mixed layer, σ_θ is nearly constant and the turbulent kinetic-energy dissipation rate ε is scaled as

$$\varepsilon(z) = 0.58J_b^o + 1.76u_*^3/kz, \quad (1)$$

where J_b^o is the surface buoyancy flux, u_* is the friction velocity related to the wind stress τ and density ρ as $u_* = (\tau/\rho)^{1/2}$, k is von Kármán's constant (= 0.41), and z is the depth of measurement (Lombardo and Gregg 1989). This scaling is expected to apply below the depths at which dissipation is influenced by surface waves (Anis and Moum 1995; Terray et al. 1996; Dren-

Corresponding author address: Dr. Douglas R. Caldwell, College of Oceanic and Atmospheric Sciences, Oregon State University, Oceanography Admin. Bldg. 104, Corvallis, OR 97331-5503.
E-mail: caldwell@oce.orst.edu

nan et al. 1996). The number of digits in the coefficients do not imply significance, only consistency with past usage by Brainerd and Gregg (1993a,b).

After dawn, restratification quiets turbulence below the wind-mixed layer and sets the stratification against which the next night's convection must work. The restratification process was studied in detail by Brainerd and Gregg (1993a,b, hereafter called BGI and BGII) at a midlatitude site (34°N, 127°W, 500 km west of Point Conception on the California coast).

At the equator also, nighttime convective turbulence drives a mixed layer in which σ_θ is nearly constant (Gregg et al. 1985; Moum and Caldwell 1985; Moum et al. 1989; Peters et al. 1988, 1994). Strong nighttime turbulence is often found, as well, below the mixed layer in always-stratified water (the ''deep cycle layer''). It is suspected that vertically propagating internal waves may be important for the generation of deep-cycle turbulence (Gregg et al. 1985; Moum et al. 1989; McPhaden and Peters 1992; Moum et al. 1992a,b; Lien et al. 1995).

In the northern-winter central equatorial Pacific, the surface boundary layer lies in the vertical shear between the surface westward-flowing South Equatorial Current and the 100-m-deep eastward-flowing Equatorial Undercurrent. This shear decreased each night in the upper 40 m to values as low as 0.001 s^{-1} (depth 20–28 m) and was restored each day to 0.006 s^{-1}. BGI observed nighttime reduction to 0.0012 s^{-1} (depth 20–40 m), but the daytime maximum they found was only 0.0022 s^{-1}.

In this paper, data obtained on a 38-day equatorial microstructure station at 140°W in November–December 1991 are analyzed to determine how the restratification process in the upper part of the surface layer differs from the midlatitude case, how the shear is restored in the daytime, and how turbulence in the deep-cycle layer decays in the daytime.

2. Construction of the composite day

Microstructure data were obtained on two overlapping Tropical Instability Wave Experiment (TIWE) cruises by *Wecoma* (Oregon State University group) and *Moana Wave* (University of Washington group). Each ship was on station at the equator at 140°W for three weeks, with a 3½ day overlap for intercalibrations. *Wecoma* was on station from 4 November to 25 November (Julian days 308–329), *Moana Wave* from 21 November to 12 December (days 325–346). The data and their processing were described by Lien et al. (1996). Data quality was examined by comparing ε measurements between the two ships (Moum et al. 1995) and by comparing Acoustic Doppler Current Profiler (ADCP) current measurements between the ships and the buoy (Lien et al. 1994).

To obtain a dataset with properties less subject to variability than the hourly series used by Lien et al. (1996), we took advantage of the remarkably stable properties of the diurnal cycle in the final 15 days of the experiment to form a composite day. (The variability was due to the inherent intermittency of turbulence and to translation of lateral variations into apparent time variations by currents and ship movement.)

This 15-day period was fairly typical of the 1990–91 period, in that the wind stress was about average, the SST was not far from the mean, and the undercurrent depth and strength were typical (Lien et al. 1995, Plate 1). The 20°C isotherm was depressed by a Kelvin wave passing through the site at the onset of an El Niño (Lien et al. 1995, Plate 2).

For the 15-day period beginning with Julian day 331.4167 (0100 local standard time, LST) the 24-hour composite day was constructed by averaging, for example, data from all casts executed from 0030 to 0130 LST as the first hour's composite. Means, medians, and 95% confidence limits were calculated for each hour at each depth by the bootstrap method, resampling the data 1400 times for the surface heat flux, wind stress, wind direction, mixed layer depth, temperature, salinity σ_θ, buoyancy frequency N, currents, shear-squared ε, the dissipation rate for temperature χ, K_h, K_ρ, and K_m. (K_h is the eddy diffusion coefficient calculated using the Cox number method as $K_h = \kappa\langle T_z^2\rangle/\langle T_z\rangle^2$, where κ is the molecular diffusivity for heat and T_z is the vertical temperature gradient. Here K_ρ is the eddy diffusion coefficient for mass, defined here as $0.2\varepsilon N^{-2}$; K_m is the eddy diffusion coefficient for momentum, defined as ε/shear^2.)

For quantities involving currents, 8-m vertically binned ship's ADCP estimates were used except for estimates at 3 and 10 m taken from buoy currents supplied by M. McPhaden and T. Dickey from the Tropical Ocean Global Atmosphere–Tropical Atmosphere Ocean (TOGA–TAO) buoy.

Profiler measurements of temperature and conductivity above 6-m depth may possibly have been affected by the presence of the ship, so the 6-m values were taken as the temperature or conductivity estimates for 5 m and above. Since the estimates for ε and χ were dubious above 13 m, again because of ship interference, the 13-m value was assigned to depths of 1–12 m (except for several calculations in which similarity estimates of ε were used and noted). For both temperature and salinity, there was in the last six days a significant trend caused by zonal advection of warm water from the western Pacific by a strong Kelvin wave (Lien et al. 1996). Because we were primarily interested in one-dimensional dynamics, in computing the temperature for the composite day we removed the trend by subtracting a depth-averaged estimate of the trend interpolated in time from vertical (6–40 m) means of 0500 LST values, that is, by removing the linear trend estimated for each day. This procedure did not change vertical gradients.

3. Properties of the composite day

After J_b^o changed from negative to positive (heat gained by water) at 0700 LST (Fig. 1a), N^2 increased

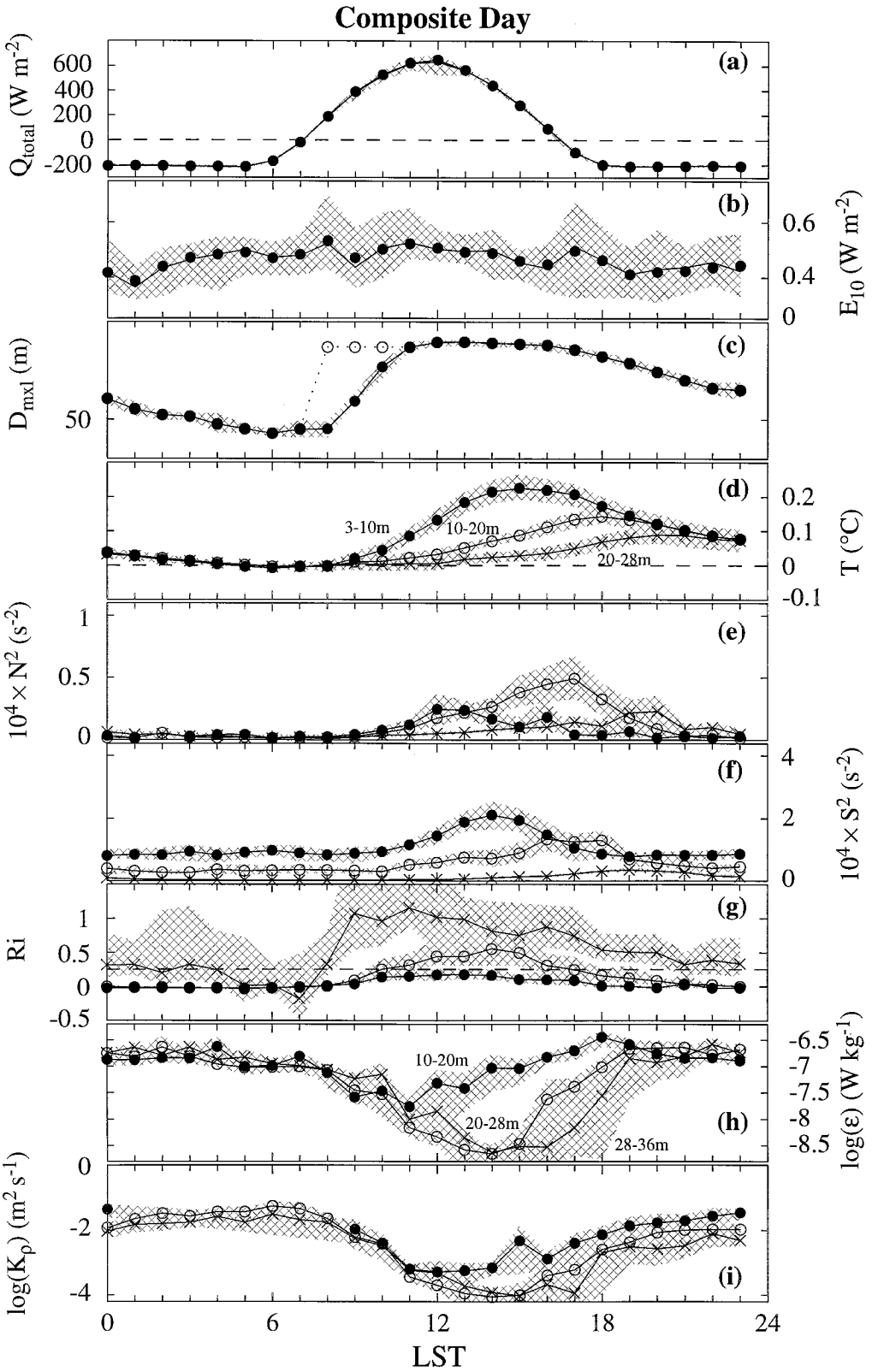

FIG. 1. Composite-day diurnal variation of (a) total surface heat flux Q_{total}, (b) wind power, E10, (c) surface mixed layer depth D_{mxl} (filled circles represent mixed layer depths determined by the $\Delta\sigma_\theta = 0.01$ criterion, open circles represent the morning mixed layer depths used in the model, as explained in the text), (d) temperature at depths 3–10, 10–20, and 20–28 m, (e) stratification N^2, (f) shear-squared S^2, and (g) Richardson number Ri, at depths 7, 16, and 24 m, (h) turbulence dissipation rate ε, and (i) turbulence diffusion coefficient K_ρ at depths 16, 24, and 32 m.

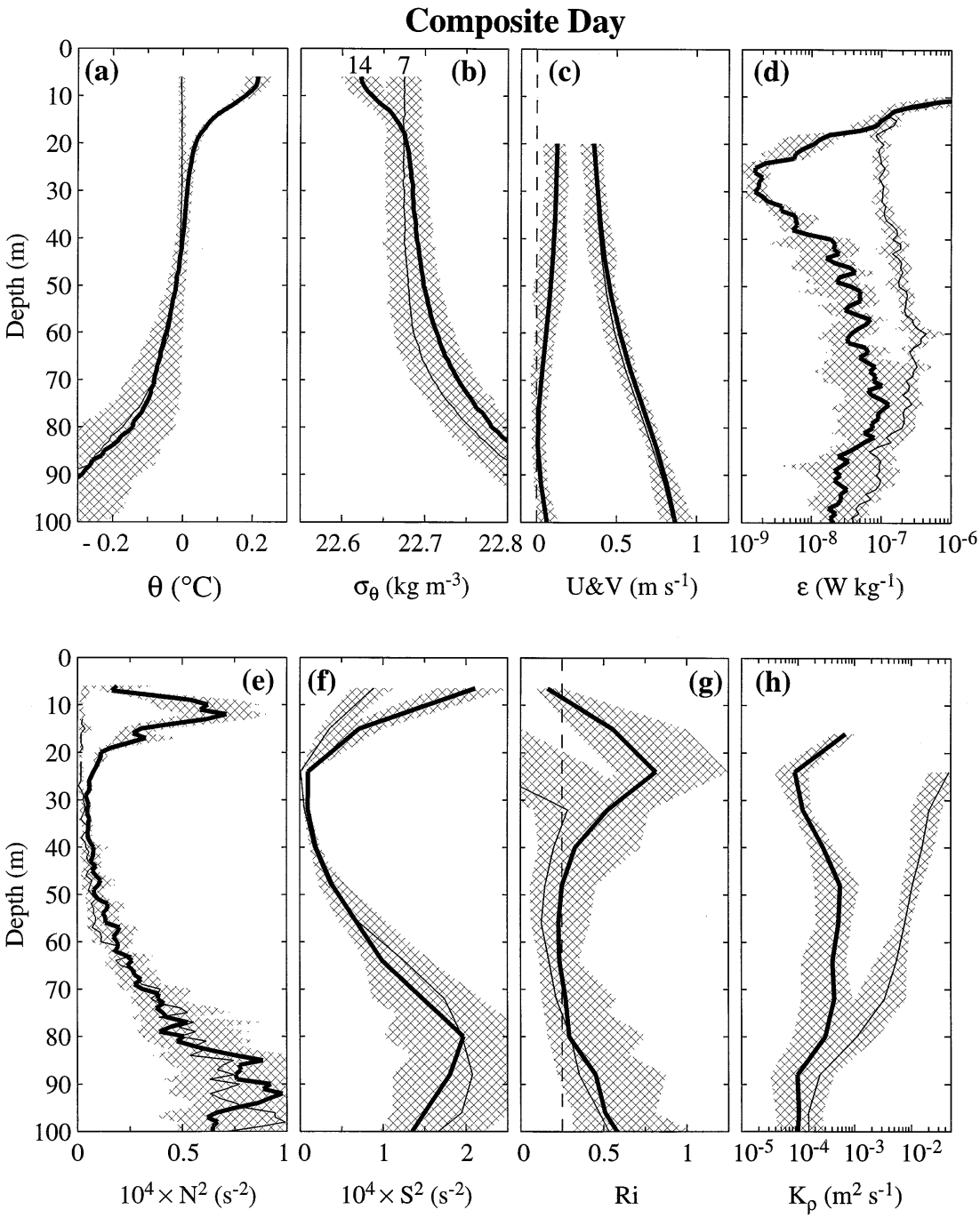

FIG. 2. Composite-day vertical profiles at 0700 LST (thin lines) and 1400 LST (thick lines) of (a) temperature θ, (b) σ_T, (c) horizontal currents [eastward (U) on right, northward (V) on left], (d) ε, (e) N^2, (f) shear-squared, (g) Richardson number, and (h) turbulent diffusion coefficient. The shading denotes the 95% confidence limits.

(Fig. 1e), more greatly at deeper depths, but the shear returned most rapidly at the surface (Fig. 1f), so that at depth 20–28 m the Richardson number Ri increased past 0.25 (Fig. 1g). Several hours later Ri (10–20 m) also increased past 0.25. As expected, ε decreased also, by almost a factor of 100 by 1400 (Fig. 1h), so did K_ρ (Fig. 1i). The diurnal thermocline, the depth at which σ_θ is greater by 0.01 than its surface value, did not retreat to its daytime value until 1100 LST, although the active mixing between 10 and 60 m declined much sooner (Figs. 1c,i). The wind power had little diurnal variation (Fig. 1b).

Comparing the composite temperature profile at 1400 LST with that at 0700 LST, it is apparent that although

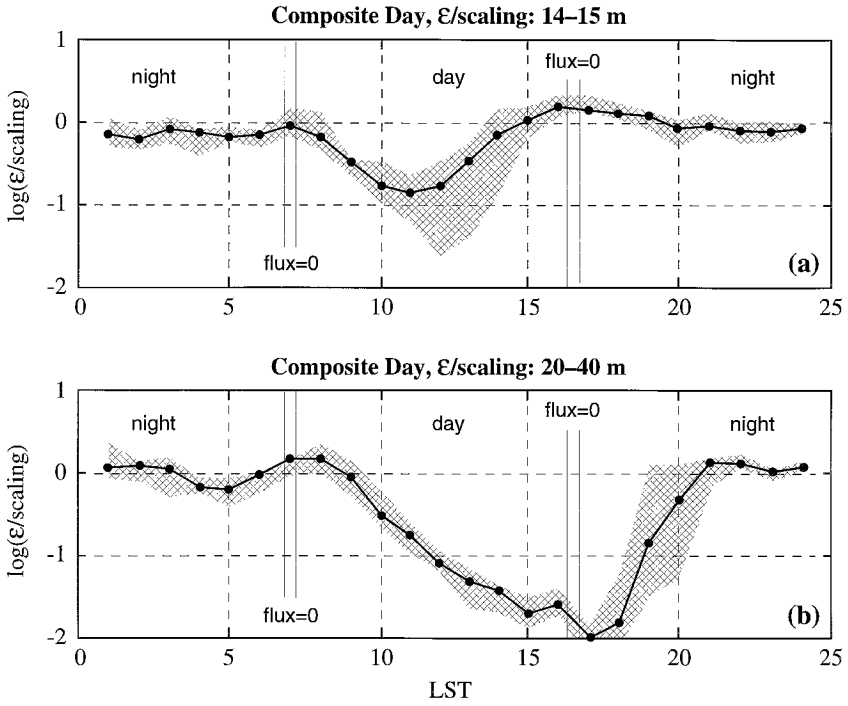

FIG. 3. Composite-day comparison of ε with the Lombardo and Gregg (1989) similarity scaling.

heating and the resultant morning increase in N^2 were confined above 40 m (Figs. 2a,e), the decrease in ε persisted to at least 70 m (Fig. 2d). Shear varied diurnally only in the top 40 m (Fig. 2f), but the diurnal change in K_ρ persisted to at least 70 m (Fig. 2h). By 1400 LST, K_ρ values throughout the surface layer are those normally typical of the thermocline.

The deep-cycle layer was found between the bottom of the nighttime mixed layer and the core of the undercurrent, with turbulence as strong as that in the mixed layer, even though the deep-cycle layer remained stratified (Fig. 2e).

4. Turbulence evolution in the remnant layer and the deep-cycle layer

The remnant layer is the water below the daytime wind-mixed layer that is within the convective mixed layer at night. The deep-cycle layer is water that is never reached by the nighttime mixed layer but that has increased levels of turbulence at night. In it, shear and N vary little from day to night.

For the composite day, ε in the nighttime mixed layer obeyed similarity scaling (1) fairly closely (Fig. 3). In the daytime, stratification decoupled most of this layer from surface forcing. This decoupling was indicated by the fact that ε at 14–15 m was smaller than the surface scaling predicted from the late morning to the late afternoon (Fig. 3a). In the 20–40-m range, ε decreased all day relative to the scaling, to a value only 1% of the similarity value, and did not recover until the nighttime convective layer again covered these depths well after dark (Fig. 3b).

One hour after the surface cooling disappeared, turbulence in the remnant layer began to decay (Fig. 4a). This one-hour time lag was approximately one period of the convective eddy, which by standard similarity scaling is $(D^2/J_b^o)^{1/3} \sim 0.9$ h, as found by BGII (D is the nighttime mixed layer depth, taken as 60 m). Then ε decreased from 10^{-7} to 10^{-9} m^2 s^{-3} (Fig. 4a). BGI observed a decrease in ε from 0.4×10^{-7} to 10^{-9} m^2 s^{-3}.

Defining the decay rate as $\tau_\varepsilon \equiv \varepsilon^{-1}\, d\varepsilon/dt$, for the composite day in the depth range 15–35 m from 0700 to 1400 LST, the 95% confidence limits for τ_ε calculated on an hourly basis were 1.1–1.5 h. For $N\tau_\varepsilon$ the 95% confidence limits were 7.2–9.3. BGI found $\tau_\varepsilon = 1.5$ h and $N\tau_\varepsilon \sim 6.0$. In an actively mixing layer suddenly isolated from surface forcing by rainfall, Smyth et al. (1997) estimated $N\tau_\varepsilon$ to be 4.3.

In the deep-cycle layer ε decayed exponentially during the daytime, but the rate was slower, the e-folding time being 3.5 h (Fig. 4b). Diurnal variations in shear and N^2 were not significant at the 95% level, and the Richardson number never significantly departed from 1/4 at the 95% confidence level.

Laboratory experiments (Stillinger et al. 1983; Itsweire et al. 1984, 1986) and ocean surface observations (Dillon 1982; Crawford 1986; Wijesekera et al. 1993; Moum 1996; Smyth et al. 1997) have found the Thorpe scale, L_T, to be a number near unity times the Ozmidov

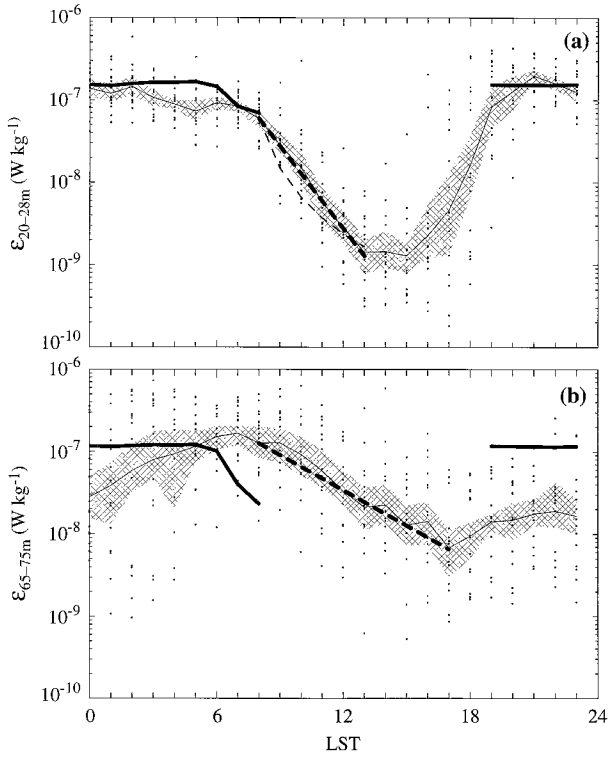

FIG. 4. Diurnal variation of epsilon in the composite day (days 331 to 346) averaged for depths of (a) 20–28 m and (b) 65–75 m. The dots represent hourly averaged data. The thin curve is the mean and the shading the 95% confidence region. The thick solid curve is the similarity scaling, which is given only for reference; it is not expected to apply at these depths. The thick dashed line is the best fit to the decay phase of observed epsilon and the thin dashed line represents the model of Brainerd and Gregg (1993b).

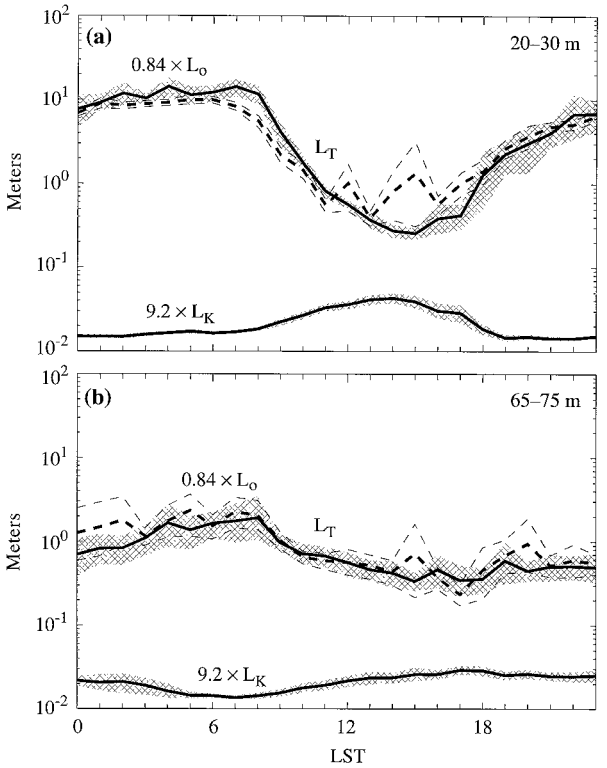

FIG. 5. Turbulence length scales averaged in (a) 20–30 m (NML) and (b) 65–75 m (DCL). The dashed curves are the mean and 95% confidence of the rms Thorpe turbulence length scale. The solid line represents $0.84L_o$, where L_o is the Ozmidov length scale, and the shading represents 95% confidence limits. At the bottom of each plot, the solid line represents $9.2L_k$, where L_k is the Kolmogorov length scale, and the shading represents 95% confidence limits.

length scale, L_O, in buoyancy-limited turbulence. [Here L_T is the rms value of the displacement of parcels of water that occurs when the parcels are sorted to make the density profile monotonic, and L_O is $(\varepsilon/N^3)^{1/2}$.]

In the composite-day remnant layer, as in BGI, as the decrease in ε and the increase in N together shortened L_O, L_T also shortened for the first decade of decay (Fig. 5a). Within the deep-cycle layer, composite-day estimates of L_T approximated L_O at all times as both varied from 0.4 to 2.0 m (Fig. 5b).

In the laboratory experiments quoted above, turbulence remained active in vertical transport, as long as L_T was more than 9.2 times the Kolmogorov length scale, $L_k \equiv (\nu^3/\varepsilon)^{1/4}$. In the composite-day remnant layer, L_T remained significantly greater than $40L_k$ and in the deep-cycle layer L_T always exceeded $90L_k$ so turbulence remained active through the day in both layers. BGI's result was the same.

The final phase of stratified turbulence decay, when restratification completely eliminates overturning eddies (Stillinger et al. 1983), was not observed in the composite day because surface cooling returned before it could occur.

Lien et al. (1996) used current meter and thermistor-chain data from the NOAA-PMEL TOGA–TAO mooring to estimate turbulence production, $\langle u'w'\rangle dU/dz$, where u' and U were determined from the 45-m current meter and w' was estimated from the high-frequency thermistor chain. This calculation was performed for a period earlier in the experiment than our composite day (because no current meter data were available for the depth of the deep-cycle layer in the later period), but at the earlier time the mixed layer was shallower so the deep-cycle layer included the 45-m depth. Production and dissipation for a composite day for this earlier period showed that shear production has about the same magnitude as ε and decays at about the same rate (Fig. 6).

5. Restratification in the remnant layer

BG's remnant layer extended from 10 m to the limit (40–60 m) of nighttime convective mixing (BGI, Fig. 11a). Its mean N^2 increased from 0.5×10^{-6} s^{-2} at dawn to a daytime maximum of 3.5×10^{-6} s^{-2}. In the equatorial composite day, the remnant layer extended from 10 to about 60 m. Its mean N^2 increased from $0.7 \times$

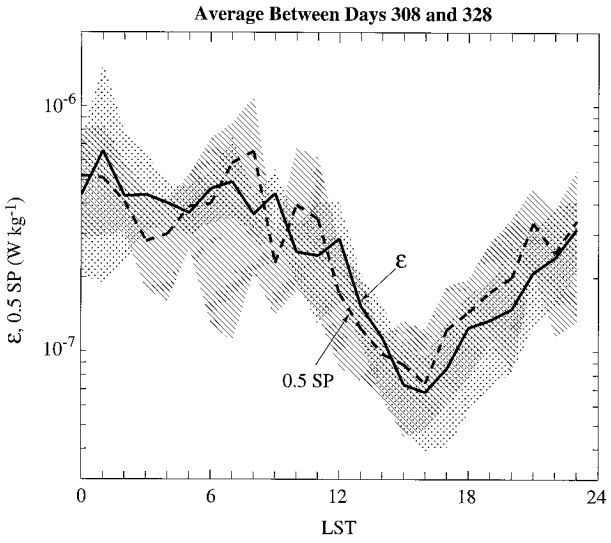

FIG. 6. Composite day of production of turbulence by shear, $\langle u'w' \rangle dU/dz$ calculated as in Lien et al. (1996), and ε calculated at 45 m for days 308–328.

10^{-6} s^{-2} at dawn to a daytime maximum of 13.3×10^{-6} s^{-2}.

BG found that the divergence of the solar flux accounted for about 60% of the restratification. Intrusions and relaxation were thought to have contributed also. Only on one day was vertical turbulent transport significant. According to BGII, ''we are left with unmeasured lateral processes as the most likely candidate for supplying the missing 40%.''

At the equator, in the top 50 m the stratification was determined almost entirely by the vertical temperature gradient. To determine how much of the restratification was caused by the divergence of the solar insolation, how much was caused by the divergence of the turbulent heat flux, and how much was due to lateral processes, we examined hour-to-hour heat budgets and constructed a simple model.

a. Heat budgets

Hourly heat budgets for the composite day were begun at 0700 LST when the heat flux first became positive (heat into the water). The shortwave heat flux was computed from the measured solar surface flux using the depth dependence of the irradiance found by Paulson and Simpson (1977) [very close to Jerlov (1968) Type 1]. Terms in the budget were calculated for various layers, with a depth-independent linear trend caused by the Kelvin wave removed from the temperature profiles, showing that, for budgets terminating at 1400 LST (Table 1):

1) The net gain in heat content from the surface to 13, 20, 40, or 60 m was larger and more variable than expected from the fluxes.
2) The divergence in the turbulent transport of heat was critically important between 13 and 20 m.
3) Below 40 m, the daily rise in heat content was not significant. Large variations in heat content below 40 m were unrelated to diurnal forcing.
4) The total heat gain could not be explained by one-dimensional fluxes. In the 0–40-m budget, the total heat gain of 561 ± 84 W m^{-2} is larger by 186 ± 68 than the sum of the fluxes. This is not caused by misestimation of radiation or turbulent transport at 40 m. Even if the solar radiation loss through the bottom (34 ± 2) and the turbulent transport through the bottom (13 ± 12) were both reduced to zero, the heat gain is still larger by 139 ± 68 than the radiative input.

b. Remnant layer restratification model

To determine the relative influences of solar flux divergence and turbulent mixing, the restratification of the remnant layer in the morning of the composite day was simulated, using composite-day estimated values (interpolated as needed) for the various quantities, such as the mixing coefficient K (estimated in several ways).

TABLE 1. Averaged daytime heat budgets for the composite day. For each day the terms were averaged from the time when the surface flux = 0 to 7 h later (0700 to 1400 LST). Ninety-five percent confidence limits determined by a bootstrap calculation with 1400 replications are given. The results were then averaged over the days. The units are watts per square meter.

Depth range (m)	Top radiative input	Top turbulent transport input	Bottom radiative output	Bottom turbulent rise in: Transport output	Bottom turbulent rise in: Heat content	Residual
0–13	419 ± 37	0	132 ± 8	116 ± 29	427 ± 65	256 ± 57
13–20	132 ± 8	116 ± 29	93 ± 6	11 ± 5	97 ± 16	−47 ± 29
20–40	93 ± 6	11 ± 5	34 ± 2	13 ± 12	64 ± 36	7 ± 34
40–60	34 ± 2	13 ± 12	13 ± 1	28 ± 26	−4 ± 46	−10 ± 44
60–80	13 ± 1	28 ± 26	5 ± 0.3	21 ± 13	14 ± 109	−2 ± 113
80–100	5 ± 0.3	21 ± 13	1.7 ± 0.1	3 ± 3	61 ± 266	40 ± 267
0–20	419 ± 37	0	93 ± 6	11 ± 5	504 ± 66	190 ± 45
0–40	419 ± 37	0	34 ± 2	13 ± 12	561 ± 84	186 ± 68
0–60	419 ± 37	0	13 ± 1	28 ± 26	556 ± 126	183 ± 98

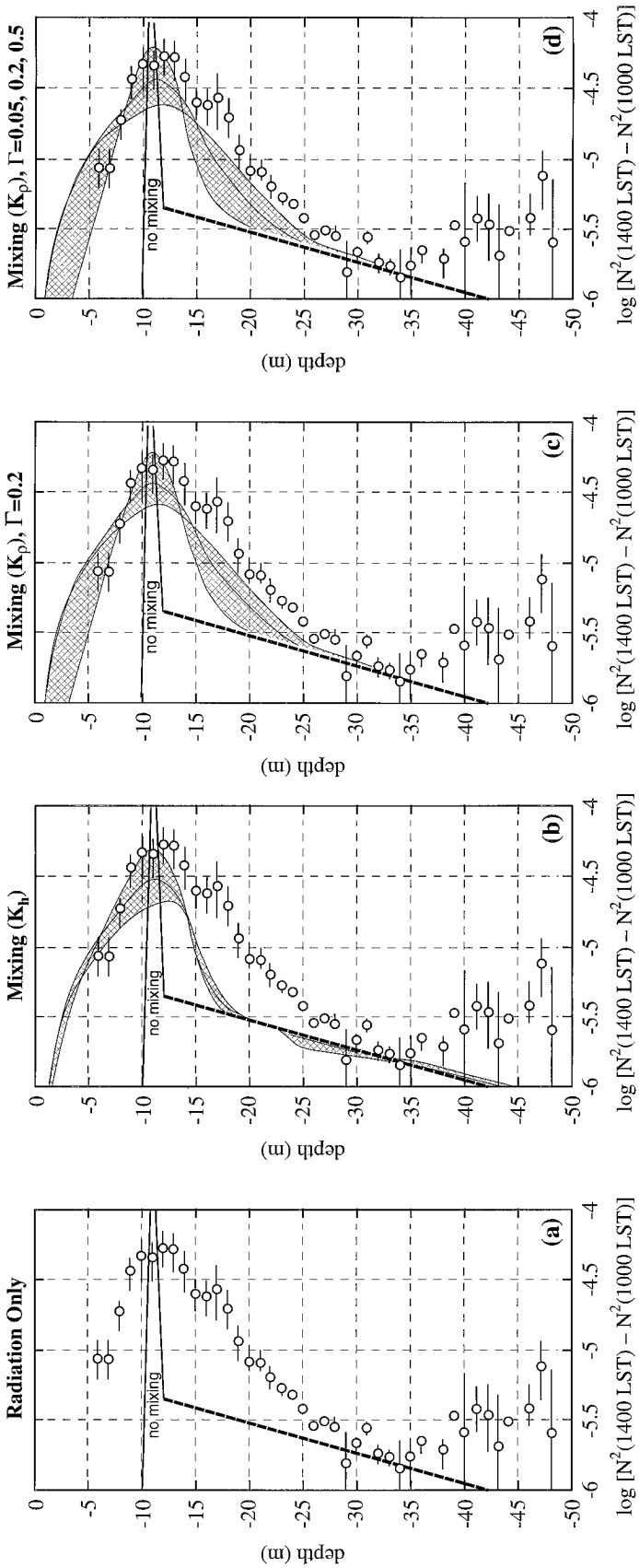

FIG. 7. Vertical profiles of N^2 for model and observations: (a) Data with 95% confidence limits is represented by open circles and lines, the prediction of the model with radiation only, no mixing is represented by the heavy dashed line. (b) As in (a) with model results including turbulent mixing with coefficient K_h. The shaded area derives from running the model with K_h set to its confidence limits. (c) As in as (b) but using K_ρ instead of K_h. (d) As in (c) but the limits of the shaded area are calculated by setting $\Gamma = 0.05$ and 0.5 in calculating K_ρ.

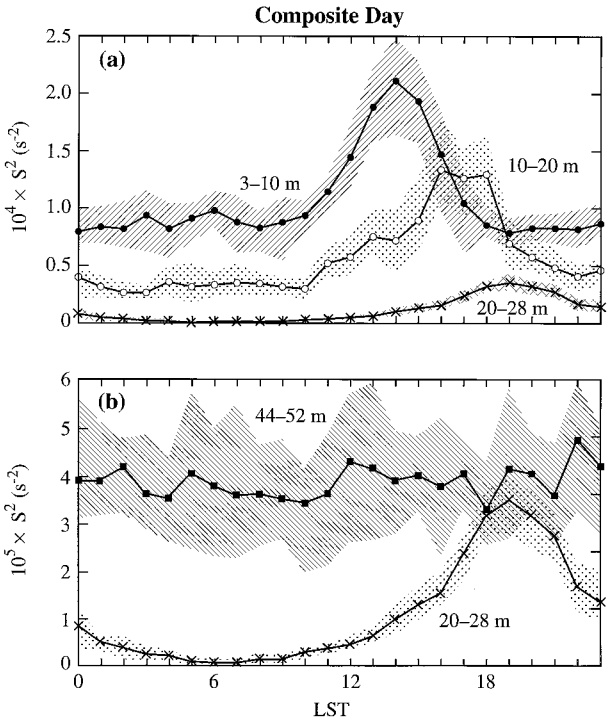

FIG. 8. Diurnal variation of shear-squared in Period II composite day (a) at depths 3–10 m, 10–20 m, and 20–28 m, and (b) at depths 20–28 m and 44–52 m. Shaded areas indicate 95% confidence limits.

The initial state was taken as the conditions at the hour during which the total surface flux J_b^o changed sign in the morning (0700 LST). The length of the time step was varied with the magnitude of the mixing coefficient, from 0.01 to 0.0001 h. Vertical resolution was 1 m. At each step, the temperature profile at time $t + \Delta t$, $T(z, t + \Delta t)$, was calculated from $T(z, t)$. Above the mixed layer depth, D_{mld}, the depth where σ_θ was 0.01 above its surface value:

$$T(z, t + \Delta t) = K\Delta t D_{zz}[T(z, t) + (\rho C_p)^{-1}(D_{\text{mld}})^{-1} \cdot (J_b^o - I(D_{\text{mld}}, t))\Delta t]. \quad (2)$$

Below the mixed layer depth

$$T(z, t + \Delta t) = K\Delta t D_{zz}[T(z, t) + (\rho C_p)^{-1} D_z I(z, t)\Delta t]. \quad (3)$$

Here $I(z, t)$ was computed as in the heat budget. We used $K(z)D_{zz}$ to approximate the flux divergence $\partial_z[K(z)\partial_z]$ because the small-scale depth dependence of the calculated $K(z)$ was large and highly subject to sampling error.

In the early morning when convection stops, the layer throughout which the surface flux is spread by large-scale motions retreats quickly to the daytime wind-mixed layer, but until the density step is rebuilt at 10 m, the σ_θ criterion yields nighttime values of D_{mld}. Therefore, we adjusted D_{mld} to return immediately to its midday value as soon as the total flux changed sign (open circles in Fig. 1c).

To maximize the response to solar heating while minimizing the effect of the arbitrariness of the early-morning D_{mld}, we compare model with data in terms of the increase of N^2 between 1000 and 1400 LST.

With no mixing ($K = 0$), restratification is due to 1) the divergence of the downward radiative flux (Fig. 7a) and 2) the step at the base of the mixed layer (N^2 too large to show on Fig. 7a). In the range 25–35 m, the model reproduces the observed N^2 fairly closely. Above 25 m it falls short. Below 35 m, other factors must dominate.

When mixing by K_h (estimated by a bootstrap calculation for the composite day as $3\kappa\langle T_z^2\rangle/\langle T_z\rangle^2$) is included, the resulting model-output N^2 resembles the observed estimates more closely above 15 m (Fig. 7b). The model was tried with values of K_h at the 2.5% and 97.5% confidence limits on the mean K_h (Fig. 7b, shaded areas). Still, the model N^2 are not nearly as large as those observed. Mixing by $K_\rho = \Gamma\varepsilon/N^2$ (computed in the same manner as K_h, with $\Gamma = 0.2$) produces N^2 closer to the observed N^2 especially in the range 15–25 m, but still, even when K_ρ at the confidence limits of the mean are used, N^2 falls short of the observed values (Fig. 7c). There is evidence that Γ may vary from the nominal value of 0.2 (Gargett and Moum 1995), so the effect of varying Γ was tried (Fig. 7d) (with mean values of ε/N^2). Here Γ close to 0.2 best simulated the observations. However, regardless of the mixing the surface fluxes provide insufficient stratification to explain the heat gain.

Summarizing the model results: From 6 to 25 m restratification is supplied by heat transported by turbulence from the wind-mixed layer and the distribution of N^2 is mainly determined by the properties of the turbulent mixing, but not all of the N^2 is explained by vertical processes. From 25 to 35 m, divergence of solar flux provides all of the restratification. Below 35 m, one-dimensional processes do not dominate. As with BGII, the observed N^2 are generally larger than predicted by one-dimensional effects; more heat is gained by the upper part of the water column than explained by the measured vertical surface fluxes.

6. Restoration of the shear in the remnant layer

At dawn, shear-squared was only 4% of its peak daytime value at 20–28 m (Fig. 8b). It was reduced to 13% at 28–36 m and 34% at 36–44 m. Below 44 m, no nighttime decrease was apparent (Fig. 8b). The 3–10- and 10–20-m shear did not decrease as much, proportionately at night (Fig. 8a). In the daytime, the shears increased again, first in the range 3–10 m, then 10–20 m, and so on. What causes the shear to reestablish itself? Possible mechanisms are

1) acceleration by the (large scale) zonal pressure gra-

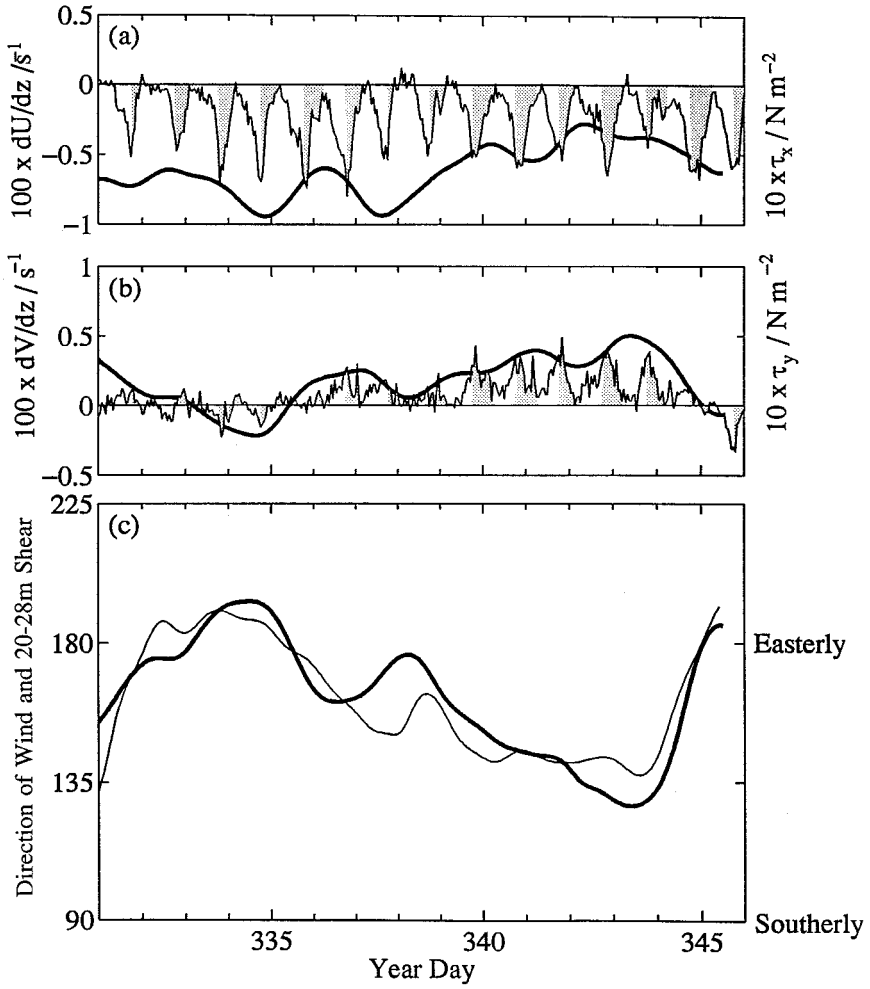

FIG. 9. Time series of (a) zonal component, (b) meridional component of velocity shear between 20 and 28 m and surface wind (thick curve), and (c) moving-average velocity shear direction (thin curve) and surface wind direction (thick curve) the time period of the composite day.

dient: The background zonal pressure gradient in this region tends to be between 2.0×10^{-7} and 6.0×10^{-7} m s^{-2} at the surface (Mangum and Hayes 1984). Its depth dependence can be represented as a Gaussian with a vertical length scale of at least 100 m (Dillon et al. 1989). Its acceleration of the surface water relative to the deeper water cannot in the course of one day produce a shear even close to the shear observed.

2) Upward turbulent transport of momentum from the mean shear below: Turbulence below 44 m is not strong enough to transport enough momentum upward to restore the shear. We expect a change in shear to propagate vertically a distance $L = (K_m t)^{1/2}$ in t s. At 40 m in the daytime, $K_m \sim 0.0003$ m^2 s^{-1}. The time for restoration of the shear is approximately 10 hours, in which time momentum from the shear below would propagate only 3 m upward.
3) Downward turbulent transport of wind stress momentum: The wind-mixed layer transports momentum down to 10 m. Below 10 m, $K_m \sim 0.01$ m^2 s^{-1} so $L \sim 19$ m, taking the momentum to 29 m, which is comparable to the depth required. If momentum from the wind were the cause, in the absence of Coriolis force the reestablished shear would lie in the direction of the wind stress, as it does (Fig. 9).

A simulation of the reestablishment of the shear was constructed to see if the estimated turbulent transport was consistent with the reestablishment of the shear in the composite day. Because the reestablished shear lay along the wind direction, the model considered currents in that direction only. At the 0700 LST an initial velocity profile with 1-m resolution was constructed by interpolating the currents from the buoy at 3-m and 10-m depth, and the ADCP currents from 20 to 84 m (Fig. 10).

At each time step, 1) the top 1 m was accelerated by the wind stress, 2) the water column was accelerated by the projected zonal pressure gradient, and 3) the velocity

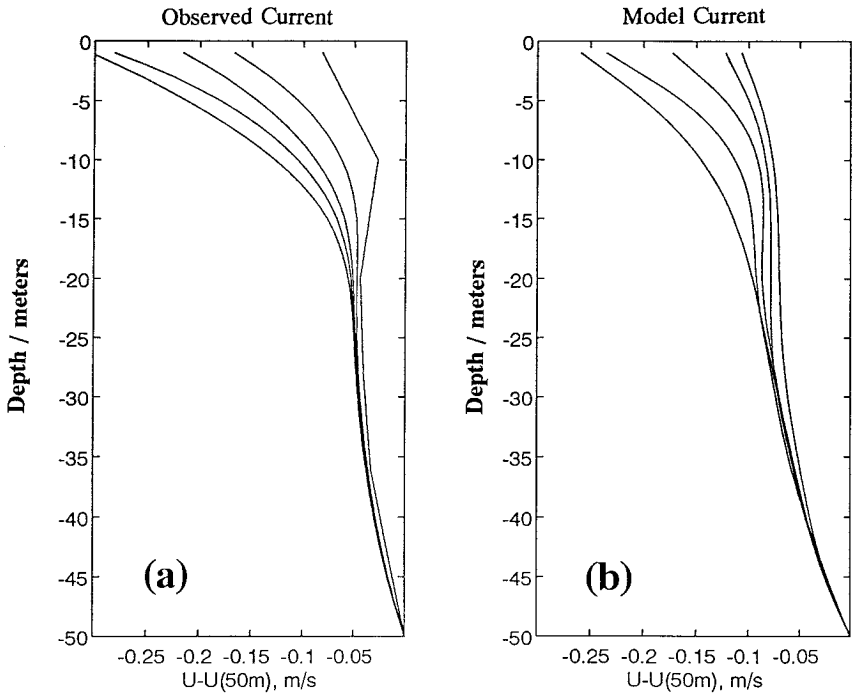

FIG. 10. Vertical profiles of (a) observed and (b) modeled currents in the wind direction for the composite day. The times of the profiles are, right to left, 0700, 0900, 1100, 1300, and 1500 LST. The currents in the wind direction at 50-m depth are subtracted from every profile.

profile was smoothed by the operator $K_m\partial_{zz}$, where K_m is the eddy mixing coefficient for momentum, estimated as $\varepsilon/(\text{shear}^2)$. Interpolated hourly mean composite-day estimates of K_m were used.

The model simulated the downwind profiles quite well (Fig. 10) and reproduced the shear-squared reestablishment at depth 20–28 m within the 95% confidence limits of the shear-squared estimates (Fig. 11). Varying parameters showed that

1) Varying the magnitude of the wind stress made only a proportionate change in the shear response. Using the observed wind stress gives the best correspondence to observations.
2) Introducing a dP/dx 100 times the estimates given by Mangum and Hayes (1984) produced no detectable effect on the shear.

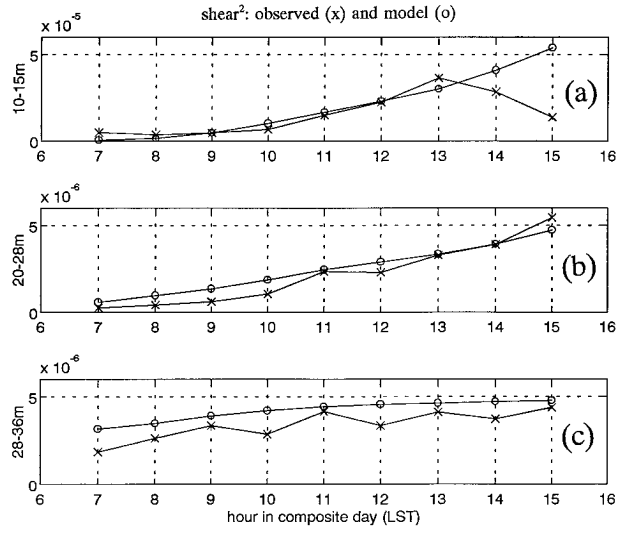

FIG. 11. Modeled and observed shear-squared vs hour in the composite day. The values are averaged over (a) 10–15 m, (b) 20–28 m, and (c) 28–36 m. The units are per square second.

7. Discussion

Why is the restratification of the remnant layer larger than can be accounted for by one-dimensional processes? In both the midlatitude case (BGII) and the equatorial case, surface and solar fluxes accounted for only 60% of the stratification gained during the day. BGII suggest that lateral processes may be responsible. Lateral variations in temperature, caused by horizontal variations in surface fluxes, may convert themselves by buoyant forces into vertical stratification. BGI (their Fig. 18) found on one night density variations (in time) of 0.01 σ_θ units. If variations are, in fact, spatial rather than temporal, they might be changed by buoyancy forces into vertical variations to account for the remaining 40% of the stratification. Over the 15-day period of our composite day, the rms deviation of each night's hourly values from each night's all-night mean was 0.023 σ_θ units. If this is interpreted as a horizontal variability and

the density difference is taken to be twice the rms deviation and if it is assumed that it is spread over 40 m vertically in the morning, the resulting N^2 is 1.1×10^{-5}, enough to supply the missing stratification.

8. Conclusions

1) For 15 days of nearly constant conditions, the day–night mixed layer cycle repeated consistently. Restratification in the remnant layer was quite similar to the process in midlatitudes observed by BG in the depth range 20–40 m in that
   (a) The minimum N at dawn was 0.5 cph compared with 0.4 cph (BG), and the peak daytime N was 2.1 cph compared with 1.1 cph (BG).
   (b) Restratification was dominated by the divergence of solar radiation from 25 to 40 m at the equator and 20 to 40 m in BG. Restratification immediately below the base of the mixed layer was dominated by turbulent mixing in the depth range 12–25 m at the equator. This region was not addressed by BG.
   (c) Turbulence decay proceeded at approximately the same rate, the e-folding time for ε being 1.7 ± 0.2 h versus 1.4 h in BG.
   (d) The length scale of the turbulence, that is, the Thorpe scale, was controlled by the Ozmidov scale in both cases.
   (e) The turbulence intensity remained well within the range of active turbulence, that is, $L_T \gg 9$ times the Kolmogoroff length scale in both cases.
2) At the equator, the shear in the remnant layer varied strongly within the diurnal cycle, both with time and depth. BG observed much smaller daytime shear.
   (a) The nighttime minima of shear-squared were $1.1 \pm 0.7 \times 10^{-6}$ s^{-2} at 20–28 m, $5.2 \pm 2.1 \times 10^{-6}$ s^{-2} at 28–36 m, and $15 \pm 7 \times 10^{-6}$ s^{-2} at 36–44 m. Shear-squared was not significantly reduced at night below 44 m. BGI found a nighttime minimum of 1.6×10^{-6} s^{-2} at 20–40 m.
   (b) The daytime maxima of shear-squared were much larger at the equator, $40 \pm 10 \times 10^{-6}$ s^{-2} at all depths from 10 to 44 m, compared with BG's 4.8×10^{-6} s^{-2} at 20 to 40 m.
   (c) The shear was reestablished by turbulent mixing of momentum transferred from the wind. The large-scale zonal pressure gradient had no measurable effect at the diurnal time scale.
3) In the deep-cycle layer, the decay was similar to the remnant layer at either midlatitude or the equator in that the turbulent scales were limited by the Ozmidov scale ($L_T \sim L_O$), as in the remnant layer, and the turbulence remained active at all times ($L_T \gg 9L_k$), but
   (a) The stratification and shear were never greatly reduced, and a diurnal variation of the Richardson number could not be demonstrated statistically at the 95% confidence level.
   (b) Decay was slower by almost a factor of 3, so production of turbulence must have nearly balanced dissipation.

Acknowledgments. This work was funded by the National Science Foundation (Grants OCE 8816098 and OCE 9314396 for the OSU portion of the work and Grants OCE 8815961 and OCE 9316004. We thank the TOGA–TAO Project Office, Michael J. McPhaden, director, for providing current meter data from the NOAA-PMEL mooring at 0°, 140°W. We also thank Keith Brainerd, Hemantha Wijesekera, David Winkel, and Clayton Paulson for helpful discussion.

REFERENCES

Anis, A., and J. N. Moum, 1995: Surface wave–turbulence interactions: Scaling $\varepsilon(z)$ near the sea surface. *J. Phys. Oceanogr.,* **25,** 2025–2045.

Brainerd, K. E., and M. C. Gregg, 1993a: Diurnal restratification and turbulence in the oceanic surface mixed layer: 1. Observations. *J. Geophys. Res.,* **98,** 22 645–22 656.

——, and ——, 1993b: Diurnal restratification and turbulence in the oceanic surface mixed layer. 2: Modeling. *J. Geophys. Res.,* **98,** 22 657–22 664.

Crawford, W. R., 1986: A comparison of length scales and decay times of turbulence in stably stratified flows. *J. Phys. Oceanogr.,* **16,** 1847–1854.

Dillon, T. M., 1982: Vertical overturns: A comparison of Thorpe and Ozmidov scales. *J. Geophys. Res.,* **87,** 9601–9613.

——, J. N. Moum, T. K. Chereskin, and D. R. Caldwell, 1989: Zonal momentum balance at the equator. *J. Phys. Oceanogr.,* **19,** 561–570.

Drennan, W. M., M. A. Donelan, E. A. Terray, and K. B. Katsaros, 1996: Oceanic turbulence dissipation measurements in SWADE. *J. Phys. Oceanogr.,* **26,** 808–815.

Gargett, A. E., and J. N. Moum, 1995: Mixing efficiencies in turbulent tidal fronts: Results from direct and indirect measurements of density flux. *J. Phys. Oceanogr.,* **25,** 2583–2608.

Gregg, M. C., H. Peters, J. C. Wesson, N. S. Oakey, and T. J. Shay, 1985: Intensive measurements of turbulence and shear in the equatorial undercurrent. *Nature,* **318,** 140–144.

Itsweire, E. G., 1984: Measurements of vertical overturns in a stably stratified turbulent flow. *Phys. Fluids,* **27,** 764–766.

——, K. N. Helland, and C. W. Van Atta, 1986: The evolution of grid-generated turbulence in a stably stratified fluid. *J. Fluid Mech.,* **162,** 299–338.

Jerlov, N. G., 1968: *Optical Oceanography.* Elsevier, 194 pp.

Lien, R.-C., M. J. McPhaden, and D. Hebert, 1994: Intercomparison of ADCP measurements at 0°, 140°W. *J. Atmos. Oceanic Technol.,* **11,** 1334–1349.

——, D. R. Caldwell, M. C. Gregg, and J. N. Moum, 1995: Turbulence variability at the equator in the central Pacific at the beginning of the 1991–93 El Niño. *J. Geophys. Res.,* **100,** 6881–6898.

——, M. J. McPhaden, and M. C. Gregg, 1996: High-frequency internal waves at 0°, 140°W and their possible relationship to deep-cycle turbulence. *J. Phys. Oceanogr.,* **26,** 581–600.

Lombardo, C. P., and M. C. Gregg, 1989: Similarity scaling during nighttime convection. *J. Geophys. Res.,* **94,** 6273–6284.

Mangum, L. J., and S. P. Hayes, 1984: The vertical structure of the zonal pressure gradient in the eastern equatorial Pacific. *J. Geophys. Res.,* **89,** 10 441–10 449.

McPhaden, M. J., and H. Peters, 1992: Diurnal cycle of internal wave

variability in the equatorial Pacific Ocean: Results from moored observations. *J. Phys. Oceanogr.*, **22,** 1317–1329.

Moum, J. N., 1996: Energy-containing scales of turbulence in the ocean thermocline. *J. Geophys. Res.,* **101,** 22 495–22 512.

——, and D. R. Caldwell, 1985: Local influences on shear flow turbulence in the equatorial ocean. *Science,* **230,** 315–316.

——, ——, and C. A. Paulson, 1989: Mixing in the equatorial surface layer and thermocline. *J. Geophys. Res.,* **94,** 2005–2021.

——, M. J. McPhaden, D. Hebert, H. Peters, C. A. Paulson, and D. R. Caldwell, 1992a: Internal waves, dynamic instabilities, and turbulence in the equatorial thermocline: An introduction to three papers in this issue. *J. Phys. Oceanogr.*, **22,** 1357–1359.

——, D. Hebert, C. A. Paulson, and D. R. Caldwell, 1992b: Turbulence and internal waves at the equator. Part I: Statistics from towed thermistors and a microstructure profiler. *J. Phys. Oceanogr.*, **22,** 1330–1345.

——, M. C. Gregg, R.-C. Lien, and M.-E. Carr, 1995: Comparison of turbulence kinetic energy dissipation rate estimates from two ocean microstructure profilers. *J. Atmos. Oceanic Technol.*, **12,** 346–366.

Paulson, C. A., and J. J. Simpson, 1977: Irradiance measurements in the upper ocean. *J. Phys. Oceanogr.,* **7,** 952–956.

Peters, H., M. C. Gregg, and J. M. Toole, 1988: On the parameterization of equatorial turbulence. *J. Geophys. Res.,* **93,** 1199–1218.

——, ——, and ——, 1989: Meridional variability of turbulence through the equatorial undercurrent. *J. Geophys. Res.,* **94,** 18 003–18 009.

——, ——, and T. B. Sanford, 1994: The diurnal cycle of the upper equatorial ocean: Turbulence, fine-scale shear, and mean shear. *J. Geophys. Res.,* **99,** 7707–7723.

Smyth, W. D., P. O. Zavialov, and J. N. Moum, 1997: Decay of turbulence in the upper ocean following sudden isolation from surface forcing. *J. Phys. Oceanogr.*, **27,** 810–822.

Stillinger, D. C., K. N. Helland, and C. W. Van Atta, 1983: Experiments on the transition of homogeneous turbulence to internal waves in a stratified fluid. *J. Fluid Mech.,* **131,** 91–122.

Terray, E. A., M. A. Donelan, Y. C. Agrawal, W. M. Drennan, K. K. Kahma, A. J. Williams, P. A. Hwang, and S. A. Kitaigorodskii, 1996: Estimates of kinetic energy dissipation under breaking waves. *J. Phys. Oceanogr.*, **26,** 792–807.

Wijesekera, H. W., T. M. Dillon, and L. Padman, 1993: Some statistical and dynamical properties of turbulence in the oceanic pycnocline. *J. Geophys. Res.,* **98,** 22 665–22 679.